sustainability

MDPI

Article

Sustainable Catalysts from Industrial FeO Waste for Pyrolysis and Oxidation of Hospital Polypropylene in Cartagena

Joaquín Hernandez-Fernandez [1,2,3,4,*], Juan Carrascal Sanchez [4] and Juan Lopez Martinez [5]

[1] Department of Natural and Exact Science, Universidad de la Costa, Barranquilla 30300, Colombia
[2] Chemical Engineering Program, School of Engineering, Universidad Tecnológica de Bolivar, Parque Industrial y Tecnológico Carlos Vélez Pombo Km 1 Vía Turbaco, Cartagena 130001, Colombia
[3] Chemistry Program, Department of Natural and Exact Sciences, San Pablo Campus, University of Cartagena, Cartagena 130015, Colombia
[4] Grupo de Investigación GIA, Fundacion Universitaria Tecnologico Comfenalco, Cr 44 D N 30A, 91, Cartagena 30015, Colombia; invest.ambiental@tecnologicocomfenalco.edu.co
[5] Institute of Materials Technology (ITM), Universitat Politecnica de Valencia (UPV), Plaza Ferrandiz and Carbonell s/n, 03801 Alcoy, Alicante, Spain; jlopezm@mcm.upv.es
* Correspondence: jhernandezf@unicartagena.edu.co

Abstract: During the COVID-19 pandemic, polypropylene waste generated in hospitals increased significantly. However, conventional strategies for the final disposal of environmental waste, such as incineration, proved inefficient due to the generation of toxic chemical species. In this research, these PP wastes were mixed with 1.5, 20, 150, 200, and 400 mg of iron oxide (FeO), extruded, and pelletized to obtain samples HW-PP-0, HW-PP-1, HW-PP-2, HW-PP-3, and HW-PP-4, respectively. XRF, TGA, and GC-MS characterized these samples. The samples were subjected to pyrolysis and thermo-oxidative degradation with controlled currents of nitrogen and oxygen. The characterization of the gases resulting from pyrolysis was carried out with a GC-MS, where the results showed that HW-PP-0 (mixed with 1.5 mg of FeO) presented the highest concentrations of alkanes (35.65%) and alkenes (63.7%), and the lowest levels of alkynes (0.3%), alcohols (0.12%), ketones (0.04%), and carboxylic acids (0.2%). The opposite was observed with the hospital waste HW-PP-4 (mixed with 400 mg of FeO), which presented the highest levels of alkynes (2.93%), alcohols (28.1%), ketones (9.8%), and carboxylic acids (8%). The effect of FeO on HW-PP-O during thermo-oxidative degradation generated values of alkanes (11%) and alkenes (30%) lower than those during pyrolysis. The results showed the catalytic power of FeO and its linear relationship with concentration. This research proposes the mechanisms that can explain the formation of different functional groups of various molecular weights which allow us to understand the presence of alkanes, alkenes, alkynes, alcohols, ketones, and carboxylic acids.

Keywords: COVID-19; hospital plastic of polypropylene waste; pyrolysis; sustainable catalyst; oxide iron; GC-MS

Citation: Hernandez-Fernandez, J.; Sanchez, J.C.; Martinez, J.L. Sustainable Catalysts from Industrial FeO Waste for Pyrolysis and Oxidation of Hospital Polypropylene in Cartagena. *Sustainability* **2024**, *16*, 5934. https://doi.org/10.3390/su16145934

Academic Editor: Grigorios L. Kyriakopoulos

Received: 4 April 2024
Revised: 26 June 2024
Accepted: 8 July 2024
Published: 11 July 2024

1. Introduction

The polymeric materials used in medical devices, such as single-use syringes, blister packaging for pills and capsules, joint replacement implants, intravenous solution bags, catheters, and cardiac assist devices, are crucial for sustaining human life [1]. The human body carries medical implants made from polymeric materials. Despite the extensive advantages of these materials, large-scale production and improper waste management have raised environmental concerns [2]. In 2018, the production of polymeric materials reached a total of 360 million metric tons (Mt), generating 7 Mt of waste (3.3 Mt corresponding to short-lived products), of which approximately 23% was incinerated, 26% was recycled, and 43% was inadequately managed [3,4]. By 2050, it is estimated that approximately 12 billion metric tons of polymeric waste will have accumulated in landfills and

the natural environment [5]; meanwhile, greenhouse gas (GHG) emissions related to the production and use of plastics are projected to account for 15% of the total global carbon budget [6]. The limited biological degradation, combined with excessive use, improper disposal, and poor management, has led to the accumulation of polymeric waste in terrestrial and aquatic areas worldwide. This accumulation impacts native wildlife and flora, agriculture, the fishing industry, and the tourism sector, while also posing a threat to human health and safety [7].

The sudden increase in the need to use polymer objects to safeguard the general population, patients, and healthcare workers is one of the severe environmental consequences of any pandemic emergency, such as the one caused by COVID-19 [8]. The widespread use of protective equipment worldwide due to the pandemic causes significant supply chain disruptions and waste management complications. It is anticipated that the demand for various polymeric products, such as personal protective equipment (PPE), including gloves and masks for healthcare workers, as well as general plastic materials like syringes, will follow the trajectory of the pandemic globally.

Polymeric items commonly used are often contaminated with pathogens and should be considered hazardous waste. Plastic waste management was already a severe environmental issue before the onset of the COVID-19 epidemic, owing to escalating concerns about pollution in terrestrial and marine ecosystems [1,9]. Global waste management systems have already faced challenges in handling current plastic waste, and the anticipated increase in waste resulting from the COVID-19 pandemic threatens to overwhelm both waste treatment systems and the capacity of healthcare services. Medical waste generated in hospitals is particularly complex due to the need to eliminate any remaining microorganisms [2,10].

Commonly, processing facilities are designed to handle conditions of stability, where medical waste is treated with uniform flow and composition. Heat-based methods such as incineration, steam sterilization (autoclaving), plasma treatment, and microwave application are employed in various treatment technologies [11]. An associated issue involves determining the optimal location for building new facilities to manage the increase in waste volume. Economic, environmental, safety, regulatory, and public acceptance issues are all factors to consider. However, these concerns arose late in the onset of the epidemic. Because these systems were designed to manage the quantity of waste generated under normal conditions, the projected volume of waste significantly exceeds the current capacity to handle hazardous medical waste [12,13].

Conventional sterilization techniques for managing COVID-19 medical waste (MW) include cremation and physical and chemical methods. These sterilization procedures are employed at various stages of waste management systems (WMSs) to handle different types of MW [14]. Cremation at high temperatures could be the most advanced or effective technology for managing chemical waste and would be an appropriate measure for decontaminating infectious and medication-related chemical waste. Although incineration technology can efficiently break down SARS-CoV-2 viruses at high temperatures, it presents certain disadvantages, such as the emission of toxins into the environment, highlighting the urgent need to develop alternatives for treating contaminated medical waste. Thermal technology has proven competent in degrading these wastes and can be classified into two main categories: pyrolysis and microwaves [15]. Pyrolysis is one of the thermal processes in which organic materials (solid and liquid waste), under oxygen-deficient conditions, decompose into smaller substances such as solid or liquid fuels, crude synthetic gases, and carbon-based materials. The resulting products have significant value in the market and can offer an energy alternative to existing fossil fuels. When subjected to pyrolysis processes, plastic waste arising during the COVID-19 crisis can generate valuable energy resources such as fluid oil, gases (synthesis gas, hydrogen), hydrocarbons, and carbon residues [15]. The liquid oil produced as one of the by-products has a high calorific value, with attributes very similar to those of any commercial fossil fuel [16].

Iron catalysts are widely used in thermal conversion due to their efficiency and low cost [17]. On the other hand, Al_2O_3 is commonly used as a support material due to its affordable price, high mechanical strength, and thermal stability [18]. For example, Jin et al. [19] demonstrated that a Fe/Al_2O_3 catalyst significantly increases hydrogen production during the catalytic decomposition of methane. Similarly, Xu et al. [20] observed that Fe/Al_2O_3 catalysts significantly enhance the oxidative dehydrogenation of ethane. Additionally, Yao et al. [21] reported that Fe-Al catalysts are effective in the thermal conversion of plastic waste, achieving high hydrogen and carbon production yields. Despite considerable efforts in plastic recycling, most research has focused on specific products such as synthesis gas [22], liquid fuels [23], the co-production of synthesis gas and carbon [24], and the generation of hydrogen and carbon nanotubes [25]. However, the relationship between the Fe/Al_2O_3 ratio and the pyrolysis behavior of plastics and the resulting products must still be fully understood. Therefore, establishing the connection between the catalyst composition and the product characteristics, and unraveling the catalytic mechanism in plastic waste pyrolysis, are crucial for improving process efficiency and product quality. The innovation of this study lies in the efficient use of FeO catalyst residues in pyrolysis to degrade the polymeric products generated during the pandemic. So far, no study has addressed this issue. Among the various catalysts used in plastic pyrolysis, those based on transition metals stand out for their capacity and partially filled 3D orbitals, which favors the dissociation of hydrocarbons through electron acceptance. Iron catalysts fit this profile, being abundant in nature and economical [26–30]. Iron oxide (FeO) has been used as a catalyst in the catalytic pyrolysis of PP [17,29,31–33]. With these catalysts, the effects of various sources of plastic waste on the quality of synthesis gas have been evaluated [34–38], and different supports have been explored to improve the efficiency of pyrolysis [39–41]. Additionally, an improvement in the production of hydrogen and nanomaterials has been observed [26,35,42–47]. FeO has also been employed in the pyrolysis of industrial virgin PP waste, generating hydrocarbon mixtures containing propylene in proportions ranging from 25.76% to 57.17% molar.

This research highlights the current COVID-19 crisis in managing, treating, and disposing of contaminated medical waste (CMW). It also seeks to provide effective solutions for the current challenges faced during COVID-19 conditions, particularly in waste management processes. The emphasis on the ecological approach of pyrolysis is of particular significance, as it could constitute an efficient treatment method for transforming CMW into valuable energy products.

2. Materials and Methods

2.1. Classification of Medical Waste and Optimal Treatment Options

Common waste comprises solid waste generated during non-medical direct activities (e.g., office waste, cafeteria waste). Infectious and potentially infectious waste is considered a subcategory of microbiology and biotechnology waste. Pharmaceutical waste belongs to the category of medications and cytotoxic drugs. Sharps waste (both used and new) includes blades, needles, scalpels, syringes, glass, and similar materials that can cause cuts or punctures. Chemical waste consists of products used in treatments or disinfection processes.

This study does not address liquid waste generated by medical activities. Radioactive sources are not used in the analyzed hospitals; therefore, such waste was not considered in the impact study.

2.2. Pyrolysis of Medical Waste: Process and Considerations

Pyrolysis is a waste combustion process carried out with a reduced oxygen content, low airflow, and relatively controlled low temperature. This method allows for the treatment of specific fractions of hospital solid waste, including infectious and pathological

materials, at extremely high temperatures ranging between 800 °C and 900 °C. The residual ashes, representing between 3% and 4% of the original mass, were properly managed in a controlled landfill to prevent soil and water contamination.

Catalytic pyrolysis experiments were conducted using thermogravimetry (TG) (NETZSCH STA 449 F3; NETZSCH Business Services GmbH, Selb, Germany) in conjunction with gas chromatography–mass spectrometry (GC-MS). Sample sizes of approximately 25 mg with diameters less than 1 mm were used. Nitrogen was injected into the reactor at a flow rate of 3 mL/min to purge the reactor and create an inert atmosphere. The reaction time for each catalytic pyrolysis experiment was set to 45 min. All these details are also described in Table 1.

Table 1. Operating conditions of the chromatograph.

Experimental Conditions of Thermogravimetric Analysis	
Temperature	**Flow**
40–900 °C. 10 °C/min	20 mL/min N_2
Experimental conditions of Chromatography	
Agilent 7820A-5975 (Agilent Technologies, Santa Clara, CA, USA)	**He Carrier: 1 mL/min**
Column #1: HP-5MS (5% PhenylMethyl Silox, 30 m × 0.25 mm I.D. × 0.25 µm), Column #2: HP-MOLESIEVE (30 m length, 0.53 mm I.D)	Oven temperature: 40 °C × 4 min, then heated to 250 °C a 10 °C/min, and 250 °C × 5 min. The split ratio is 10:1. S source and MS quad are 230 and 150 °C.
Experimental conditions of thermogravimetric analysis	
Temperature	**Flow**
40–900 °C. 10 °C/min	20 mL/min N_2
Experimental conditions of Chromatography	
Agilent 7820A-5975	**He Carrier: 1 mL/min**
Column #1: HP-5MS (5% PhenylMethyl Silox, 30 m × 0.25 mm I.D. × 0.25 µm), Column #2: HP-MOLESIEVE (30 m length, 0.53 mm I.D)	Oven temperature: 40 °C × 4 min, then heated to 250 °C a 10 °C/min, and 250 °C × 5 min. The split ratio is 10:1. S source and MS quad are 230 and 150 °C.

The resulting solid waste, after treatment, is inert and is deposited in landfills. Due to the controlled conditions of combustion, pyrolysis is more manageable than incineration and is often preferred for waste treatment in developed countries, according to the literature.

2.3. Sampling of PP Hospital Waste (HPW)

The HPW was sampled during the pandemic, specifically between June and December 2021, in a hospital in the north of Cartagena-Colombia. The samples were delivered by the competent clinic staff and treated using the safety protocols designed by the Colombian government. They were washed with steam, dried at room temperature, ground to a mesh size of 120 microns, and dried in an oven at 80 °C. The HPW was divided into five samples of 1 kg each. See Table 2.

Table 2. Sample processing conditions.

HPW Samples	HPW (kg)	Washing	FeO (mg)
HW-PP-0	1	steam water	1.5
HW-PP-1	1	steam water	20
HW-PP-2	1	steam water	150
HW-PP-3	1	steam water	200
HW-PP-4	1	steam water	400

Samples HW-PP-0 to HW-PP-4 were independently premixed with 1.5, 20, 150, 200, and 400 mg FeO. A standard Prodex Henschel 115JSS mixer (Perry (Hainesport, NJ, USA)) was used to homogenize the mixtures at 800 rpm for 7 min at room temperature. Subsequently, the samples were mixed by melt-extrusion using a Welex-200 24.1 extruder (KD Capital Equipment, LLC, Scottsdale, AZ, USA). The extruder temperatures were 190, 195, 200, 210, 210, and 220 °C. See Figure 1.

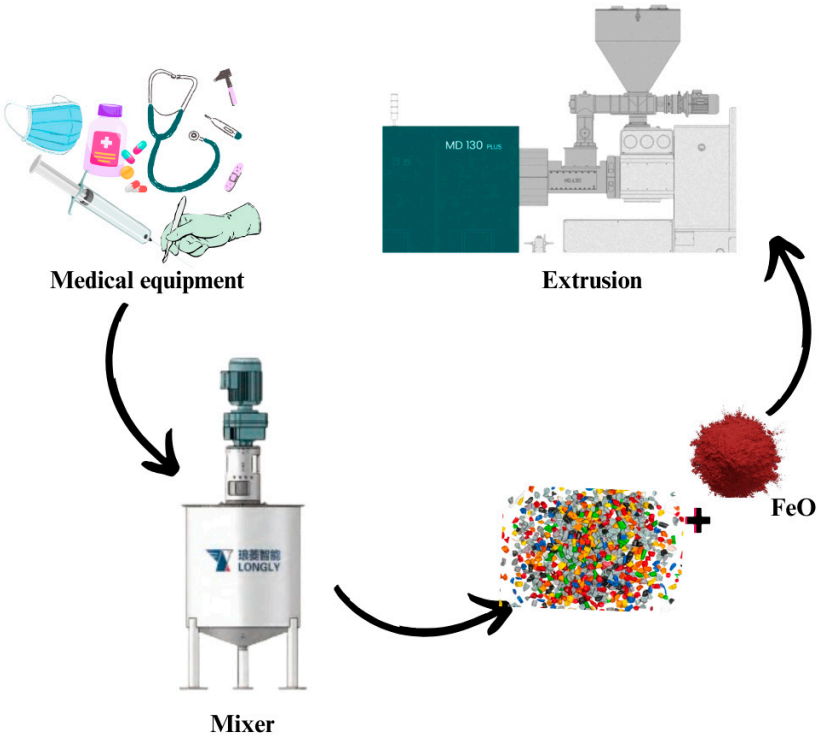

Figure 1. Processing diagram.

2.4. Humidity

With a Vapor ProXL Computrac (BROOKFIELD AMETEK, Middleborough, MA, USA), the HPW samples were examined for moisture content. HPW samples of 5 g were filled into a 25 mL glass vial.

2.5. XRF (X-ray Fluorescence)

The Axios FAST elemental analyzer (Malvern Panalytical Ltd., Malvern, UK) and the Zetium polymer editing elemental analyzer from Malvern Panalytical were used to perform X-ray fluorescence analysis of metal residues produced during catalysis [48].

2.6. MFI (Melt Flow Rate)

The melt flow index was determined using a Tinius Olsen MP1200 (MFI) plastometer (Imocom S.A. Columbia, Bogota, Colombia, S.A.). A 2.16 kg piston was used to move the melt when the internal temperature of the plastometer barrel was 230 °C [49].

2.7. TGA (Thermal Gravimetric Analysis)

A Perkin Elmer TGA 7 thermobalance (Artisan Technology Group® 101 Mercury Drive, Champaign, IL, USA) was used to perform thermogravimetric analysis (TGA). The samples weighed between 18 and 22 mg. In the experiments, the samples were heated from 30 to 700 °C at a continuous rate of 10 °C per minute while being exposed to nitrogen at a flow rate of 50 mL per minute. It was derived from the TGA curve as the temperature

at 5 percent weight loss, and the maximum degradation temperature was derived from the DTG curve.

2.8. Analysis of Variance (ANOVA) and Error

Data analysis was performed using Minitab 18 statistical analysis software© 2024 for scientific data. An ANOVA of a single response factor (Mass %) was performed, using Tukey's grouping method with 95% confidence and $\alpha = 0.05$. The parameters associated with the error of this analysis, such as sum of squares of the error (Adjusted SC) and mean of squares of the error (Adjusted MC), were automatically calculated by the software.

3. Results and Discussion

3.1. Elemental, Proximal, and Final Analysis

Table 3 shows the elemental composition of HW-PP-0, HW-PP-1, HW-PP-2, HW-PP-3, and HW-PP-4. No significant differences in volatiles, ashes, carbon, nitrogen, oxygen, Ti, Al, or Cl compositions are observed. These measurements allowed us to demonstrate the amounts of Fe added and to show that although FeO is not added to HW-PP-0, this contains 1.16 mg kg^{-1}, which must be associated with the origin of the same sample. The rest of the samples show the expected trends.

Table 3. Mass percentages of aggregation states and elements of the HPW samples.

Feed	HW-PP-0	HW-PP-1	HW-PP-2	HW-PP-3	HW-PP-4
Proximate analysis (as received)					
Moisture, wt%	0.15	0.27	0.33	0.32	0.39
Volatile matter, wt%	99.7	99.53	99.51	99.43	99.32
Fixed carbon, wt%	0.11	0.13	0.13	0.18	0.09
Ash, wt%	0.04	0.07	0.03	0.07	0.2
Ultimate analysis (as received, wt%)					
C, wt%	84.15	84.73	84.25	84.99	83.87
H, wt%	14.4	13.9	14.07	13.43	14.56
N, wt%	0.07	0.05	0.09	0.07	0.05
S, wt%	0.32	0.39	0.41	0.47	0.41
O, wt%	1.06	0.95	1.18	1.04	1.11
Ti, mg kg^{-1}	0.46	0.46	0.46	0.46	0.46
Al, mg kg^{-1}	5.23	6.23	7.33	8.21	7.13
Cl, mg kg^{-1}	12.6	11.42	11.21	12.11	12.93
Fe, mg kg^{-1}	1.16	15.55	116.59	155.46	310.92

3.2. TGA (Thermal Gravimetric Analysis)

The TGA (A) and DTGA (B) curves are shown in Figure 2. The FeO concentrations added were 1.5, 20, 150, 200, and 400 ppm. The thermograms of the PP samples showed a behavior indicated in the bibliography [34,35,50,51] at a heating rate of 20 C min^{-1}. The results of all tests indicate a higher degree of degradation for samples containing more FeO. The PP materials with the least amount of FeO presented the highest thermal stability. As the FeO concentration increases, the TG and DTG curves of PP hospital waste change. The sample with the highest FeO content (400 ppm) presents a significant change in the curve near 150 °C, with a maximum mass loss rate of 23.52% $°C^{-1}$ at approximately 441 °C. The sample with the lowest FeO content (1.5 ppm) presents a significant change in the degradation curve above 400 °C with a minimum rate of 14.98% $°C^{-1}$.

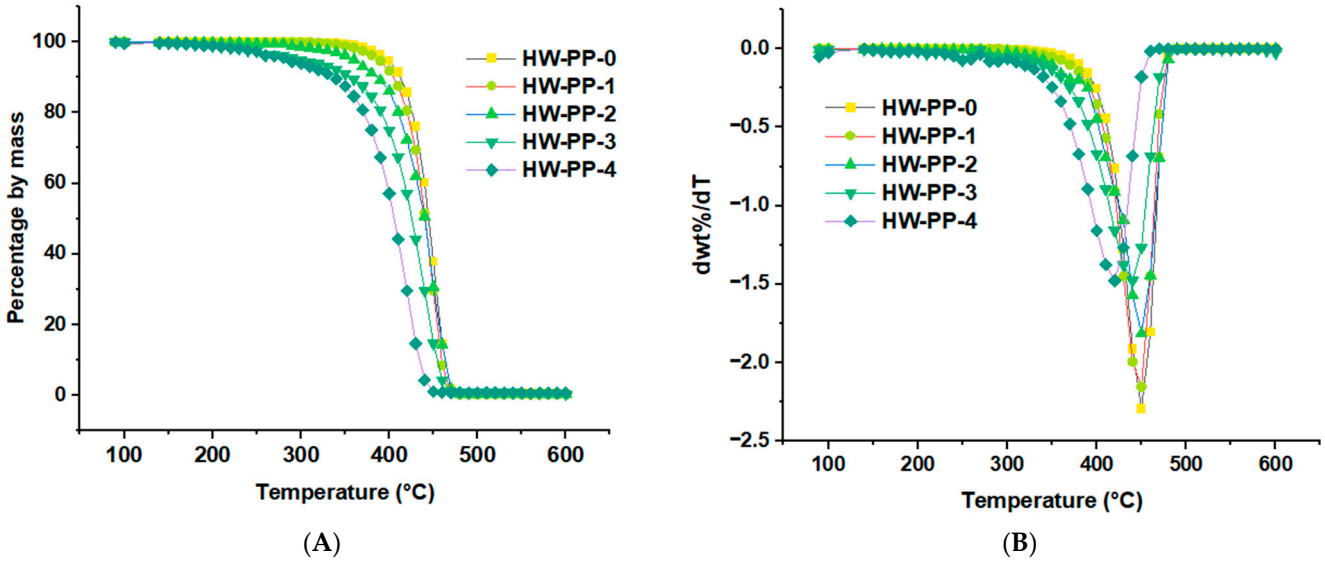

(**A**) (**B**)

Figure 2. TGA (**A**) and dTGA (**B**) for PP with different amounts of iron oxide.

Temperature

The temperature plays a crucial role in pyrolysis, particularly in the breakdown of the plastic's polymer chain. The ideal temperature regulates this process. As the temperature increases, the molecules of the materials start to vibrate and tend to evaporate from the surface. This occurs when the energy induced by van der Waals forces along the polymer chains increases, surpassing the enthalpy of the single C–C bond, causing the carbon chain to break [52,53]. Additionally, higher operating temperatures in pyrolysis yield better results for non-condensable gases (syngas, synthetic gas), while lower temperatures are recommended to achieve higher yields of solid products, such as charcoal, biochar, and coke.

Harussani et al. [54] investigated the effect of temperature on the decomposition phase of PP. According to thermal analysis, the decomposition of PP began at 400 °C, as reported by Marcilla et al. [55]. Theoretically, PP decomposes more rapidly than other polyolefins because half of the carbon in the PP chain is tertiary carbon, which facilitates the production of tertiary carbocations during decomposition [56]. Panda et al. [57] explained that this phenomenon occurs due to the recombination of byproducts through a regressive rearrangement, leading to char formation. Thus, coke and carbon formation are greater than liquid products in this phase, at 5.7% at 400 °C. However, the maximum char yield occurred at a low temperature of 250 °C, with 13.68% of solid residue collected. Ahmad et al. [58] studied the effect of temperature on the thermal cracking of polyolefin polymers, PP, and HDPE. As the temperature increased, the total yield rose from 86% at 250 °C to 99% at 300 °C. This suggests that PP decomposes quickly due to its branched structure and the higher proportion of tertiary carbons in its polymer chains, which leads to the thermal cleavage of C–C bonds [59]. However, the conversion decreased as the process temperature increased from 300 to 350 °C.

3.3. Pyrolysis

3.3.1. Alkanes

In the pyrolysis of the five samples of PP waste, 30 compounds were identified, with functional groups of alkanes, alkenes, alkynes, alcohols, ketones, and acids. Seven alkanes, made up of C1 to C5, were identified. Methane was the most straightforward organic substance with concentrations ≤5%. This showed a decreasing variation regarding the presence of FeO. In the samples with 1.5 ppm FeO, 5% methane was found, and for the sample with 400 ppm FeO, 1.1% methane was found. The ethane content was ≤12.1%. For the

sample with 1.5 ppm FeO, 12.1% ethane was obtained, and for the sample with 400 ppm FeO, 1.6% ethane was obtained. Propane presented levels ≤3.6%. Isopentane presented percentages ≤13.5% and, like methane, gave a continuous decrease in all the samples studied. Figure 3a graphically shows what has been described. The ANOVA analysis (Table 4) for the alkanes shows that for isopentane and ethane, there are no significant differences between their means, the same as for ethane, methane, and propane, and there are no significant differences between methane, propane, N-butane, cyclopropane. Because they are actual data treated statistically, the transitivity principle still needs to be fulfilled. Figure 4a complements the information in Table 4.

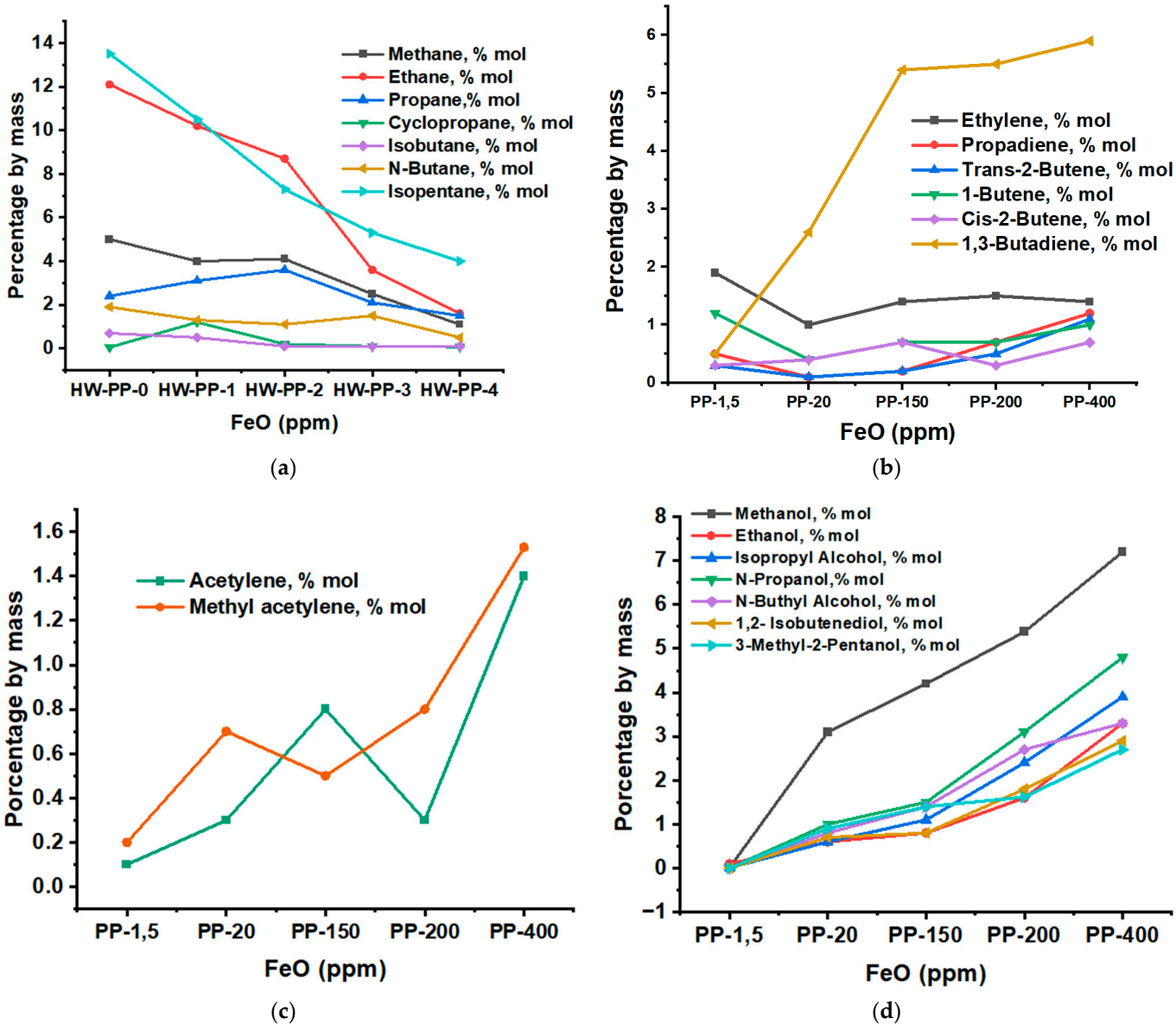

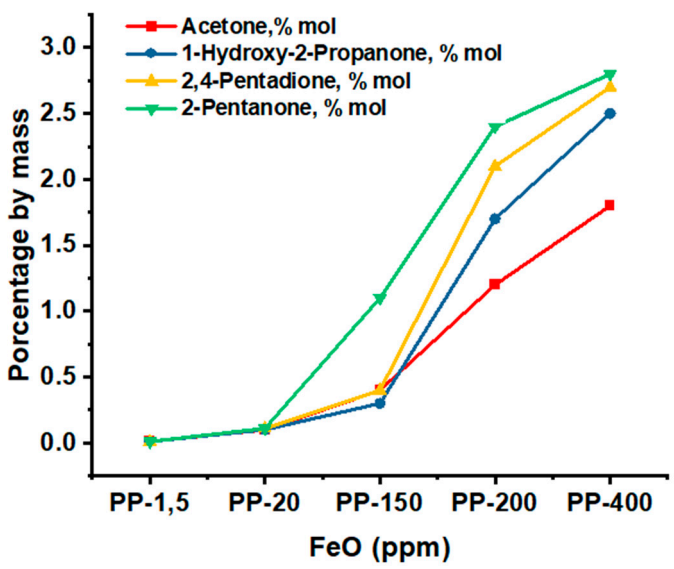

(**e**)

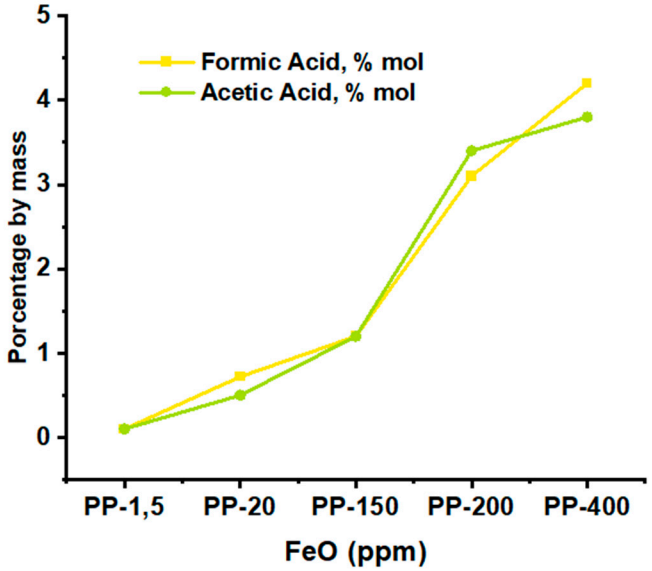

(**f**)

Figure 3. (**a**) Trend graph for alkanes as a function of the amount of FeO; (**b**) trend graph for alkenes as a function of the amount of FeO; (**c**) trend graph for alkynes as a function of the amount of FeO; (**d**) trend graph for alcohols as a function of the amount of FeO; (**e**) trend graph for ketones as a function of the amount of FeO; (**f**) trend graph for acids as a function of the amount of FeO.

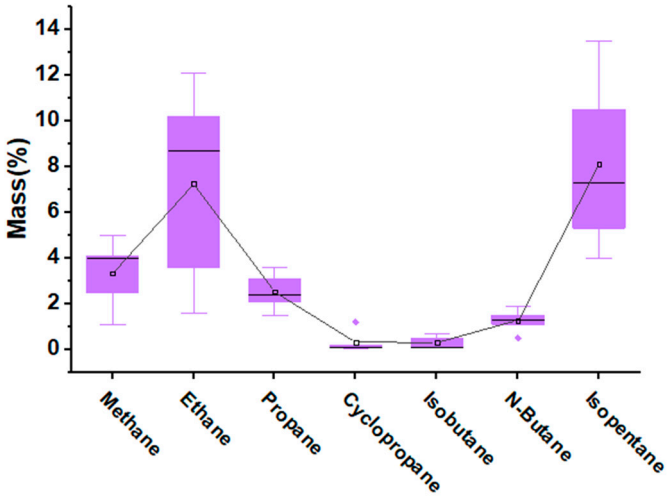

(**a**)

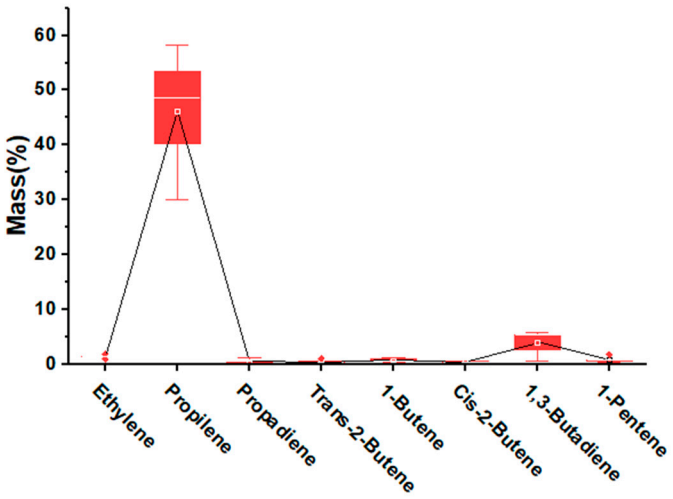

(**b**)

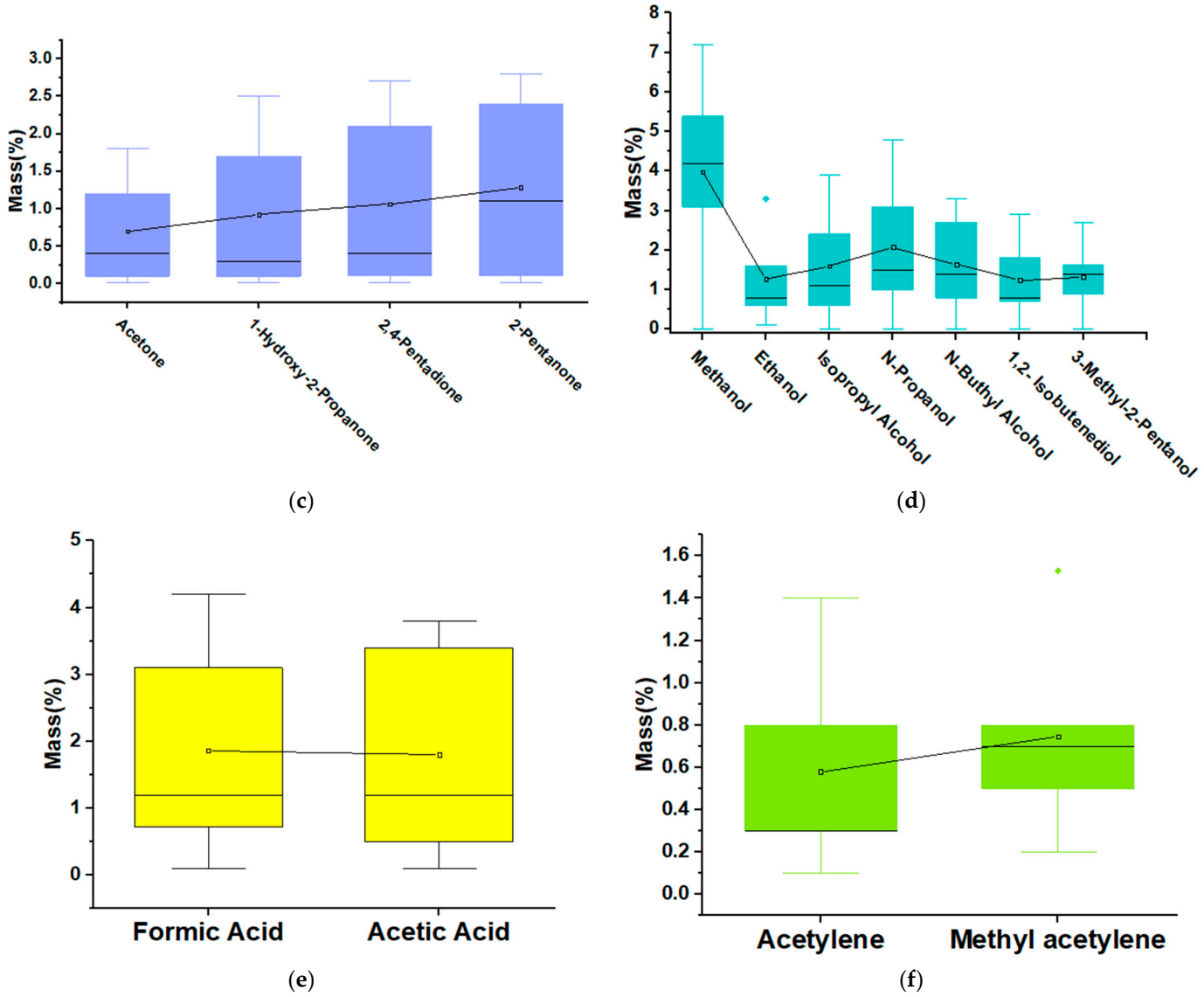

Figure 4. (**a**) Boxplot for alkanes; (**b**) boxplot for alkenes; (**c**) boxplot for ketones; (**d**) boxplot for alcohols; (**e**) boxplot for acids; (**f**) boxplot for alkynes.

Table 4. Set of ANOVA analyses for states and family of compounds.

ANOVA of Proximal Analysis					
Factor	**N**	**Average**	**Grouping**	**SC Adjusted Error**	**MC Adjusted Error**
Moisture, wt%	5	0.292	A		
Fixed carbon, wt%	5	0.128	B	0.055	0.004637
Ash, wt%	5	0.082	B		
ANOVA for Alkanes					
Isopentane, % mol	5	8.12	A		
Ethane, % mol	5	7.24	A B		
Methane, % mol	5	3.34	B C		
Propane, % mol	5	2.54	B C	154.4	5.513
N-Butane, % mol	5	1.26	C		
Cyclopropane, % mol	5	0.324	C		
Isobutane, % mol	5	0.3	C		
ANOVA for Alkenes					
Propylene % mol	5	46.16	A		
1,3-Butadiene, % mol	5	3.98	B	526.6	16.45
Ethylene, % mol	5	1.44	B		

1-Pentene, % mole	5	0.94	B		
1-Butene, % mol	5	0.8	B		
Propadiene, % mol	5	0.54	B		
Cis-2-Butene, % mol	5	0.48	B		
Trans-2-Butene, % mol	5	0.44	B		
ANOVA for Alkynes					
Methyl acetylene, % mol	5	0.746	A	2.086	0.261
Acetylene, % mol	5	0.58	A		
ANOVA for Alcohols					
Methanol, % mol	5	3.98	A	75.50	2.696
N-Propanol, % mol	5	2.08	A		
N-Butyl Alcohol, % mol	5	1.64	A		
Alcohol Isopropyl, % mol	5	1.602	A		
3-Methyl-2-Pentanol, % mol	5	1.324	A		
Ethanol, % mol	5	1.28	A		
1,2- Isobutenediol, % mol	5	1.24	A		
ANOVA for Ketones					
2-Pentanone, % mol	5	1.284	A	20.16	1.266
2,4-Pentadione, % mol	5	1.064	A		
1-Hydroxy-2-Propanone, % mol	5	0.922	A		
Acetone, % mol	5	0.702	A		
ANOVA for Acids					
Formic Acid, % mol	5	1.864	A	23.34	2.918
Acetic Acid, % mol	5	1.8	A		

Alkenes

For the alkenes, like the alkanes, products with the same number of carbons (C2–C5) were found. Ethylene presented concentrations ≤1.9%. Propylene was the product obtained in greater quantity with values ≤58.3%. For propadiene, trans-2-butene, 1-Butene, Cis-2-butene, and 1-pentene, their concentrations were ≤1.8%. For 1,3-Butadiene, its levels were ≤5.9%. The above can be observed graphically in Figure 3b. The ANOVA analysis for the alkenes in Table 4 does not show significant differences between the products, except propylene. Figure 4b shows the box-and-whisker plot for the alkenes, which graphically corroborates important differences.

Alkynes

Only two products were obtained for the alkynes, with the lowest presence in general terms concerning the other families of compounds. One of them was acetylene or ethyne, with values ≤1.4%. The other alkyne, methyl-acetylene or 1-propyne, presented values ≤1.53%. Everything described above can be seen graphically in Figure 3c. Contrary to alkanes and alkenes, alkynes tend to increase their presence in the products they produce. The ANOVA analysis for the alkynes in Table 4 indicates no significant differences between the two products obtained, corroborated in Figure 4f.

Alcohols

For this family, eight compounds, like the alkanes, had between 1 and 5 carbons (C1–C5). In addition, a polyfunctional combination (1,2-isobutene-diol) with two hydroxyl groups (OH) and one alkene group (C=C) was found in this family. For this family, carrying out the substance-by-substance analysis is not optimal since they all presented the same behavior, indicating a direct influence of FeO. The most abundant alcohols (greater than 4%) were methanol and N-propanol. These results open the possibility of going deeper into similar studies in the future that demonstrate the feasibility of establishing production processes for alcohols and other oxygenated families using FeO in the pyrolysis of PP. Figure 3d shows the general trend by substance and by family in the percentage

growth of the products as a function of the amount of FeO. The ANOVA analysis for the alcohol family showed that, in general, there are no significant differences in their means, as shown in Table 4 and Figure 4d. Table 5 shows all the products obtained by pyrolysis categorized by families.

Table 5. Percentage weight values for the species recorded by GC-MS.

Composts (Pyrolysis)	**Samples**				
	HW-PP-0	**HW-PP-1**	**HW-PP-2**	**HW-PP-3**	**HW-PP-4**
Alkanes					
Methane, % mol	5	4	4.1	2.5	1.1
Ethane, % mol	12.1	10.2	8.7	3.6	1.6
Propane, % mol	2.4	3.1	3.6	2.1	1.5
Cyclopropane, % mol	0.05	1.2	0.2	0.1	0.07
Isobutane, % mol	0.7	0.5	0.1	0.1	0.1
N-Butane, % mol	1.9	1.3	1.1	1.5	0.5
Isopentane, % mol	13.5	10.5	7.3	5.3	4
Total Amount	35.65	30.8	25.1	15.2	8.87
Alkenes					
Ethylene, % mol	1.9	1	1.4	1.5	1.4
Propylene % mol	58.3	53.5	48.7	40.2	30.1
Propadiene, % mol	0.5	0.1	0.2	0.7	1.2
Trans-2-Butene, % mol	0.3	0.1	0.2	0.5	1.1
1-Butene, % mol	1.2	0.4	0.7	0.7	1
Cis-2-Butene, % mol	0.3	0.4	0.7	0.3	0.7
1,3-Butadiene, % mol	0.5	2.6	5.4	5.5	5.9
1-Pentene, % mole	0.7	0.8	0.5	1.8	0.9
Total Amount	63.7	58.9	57.8	51.2	42.3
Alkynes					
Acetylene, % mol	0.1	0.3	0.8	0.3	1.4
Methyl acetylene, % mol	0.2	0.7	0.5	0.8	1.53
Total Amount	0.3	1	1.3	1.1	2.93
Alcohols					
Methanol, % mol	0.01	3.1	4.2	5.38	7.2
Ethanol, % mol	0.1	0.6	0.8	1.6	3.3
Alcohol Isopropyl, % mol	0.01	0.6	1.1	2.4	3.9
N-Propanol, % mol	0	1	1.5	3.1	4.8
N-Butyl Alcohol, % mol	0	0.8	1.4	2.7	3.3
1,2- Isobutenediol, % mol	0	0.7	0.8	1.8	2.9
3-Methyl-2-Pentanol, % mol	0	0.9	1.4	1.62	2.7
Total Amount	0.12	7.7	11.2	18.6	28.1
Ketone					
Acetone, % mole	0.01	0.1	0.4	1.2	1.8
1-Hydroxy-2-Propanone, % mol	0.01	0.1	0.3	1.7	2.5
2,4-Pentadione, % mol	0.01	0.11	0.4	2.1	2.7
2-Pentanone, % mol	0.01	0.11	1.1	2.4	2.8
Total Amount	0.04	0.42	2.2	7.4	9.8
Acids					
Formic Acid, % mol	0.1	0.72	1.2	3.1	4.2
Acetic Acid, % mol	0.1	0.5	1.2	3.4	3.8
Total Amount	0.2	1.22	2.4	6.5	8
Total	100.01	100.04	100	100	100

Ketones

For the ketones, we obtained the same behavior as for the alcohols, as shown in Table 5. The highest values were for 2,4-pentadione and 2-pentanone, with 2.7% and 2.8%, respectively. Bifunctional compounds such as 1-Hydroxy-2-propanone and 2,4-propanone were found. All this is shown in Figures 3e and 4c. Table 4 shows the ANOVA analysis; as in alcohols, there are no significant differences in their means.

Acids

Just like the alkynes, only two products were obtained for this family, as shown in Figure 3f. In the case of these substances, only those corresponding to C1 and C2 in their structure were recorded. Table 4 shows the ANOVA analysis for the family of acids, in which it is understood that there are no significant differences in the percentage means of these species. Figure 4e graphically corroborates the results of Table 5.

3.3.2. Thermal Oxidation

Figure 5 shows the differences in the behavior of PP hospital waste when in the presence of an inert environment, another oxidative, and with a catalyst such as FeO in different concentrations. The graphs (Figure 6) presented illustrate the thermal degradation of alkanes, alkenes, alkynes, acids, ketones, and alcohols under inert (N_2) and oxidative (O_2) atmospheres. The results show that in an inert atmosphere, the mass of alkanes and alkenes decreases significantly as degradation progresses, with a more pronounced reduction in alkanes. In contrast, under an oxidative atmosphere, the decrease in mass is less notable for alkanes and shows variability in alkenes, with a mass recovery in samples HW-PP-3 and HW-PP-4. Figure 4d–f show that the percentage of mass of these compounds increases with the sample number in both atmospheres. However, significant differences are observed between the two environments: the oxidative atmosphere promotes excellent formation of ketones, reaching a significantly higher percentage of mass compared to the inert atmosphere in sample HW-PP-4.

On the other hand, degradation in an inert atmosphere favors the accumulation of alcohols, showing a notable increase compared to the oxidative atmosphere, especially in HW-PP-4. Acids exhibited similar behavior in both atmospheres up to HW-PP-3, with a slight predominance in the inert atmosphere in HW-PP-4. Figure 7 graphically summarizes the products obtained.

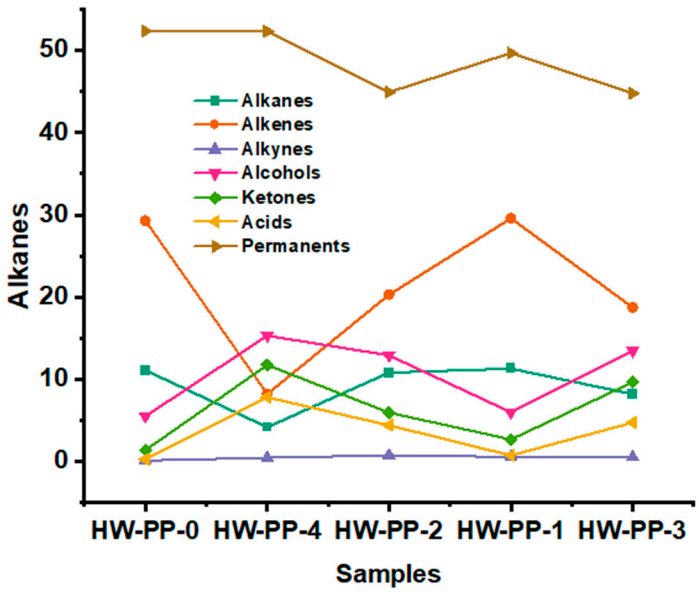

Figure 5. Trends by families in an oxidative atmosphere.

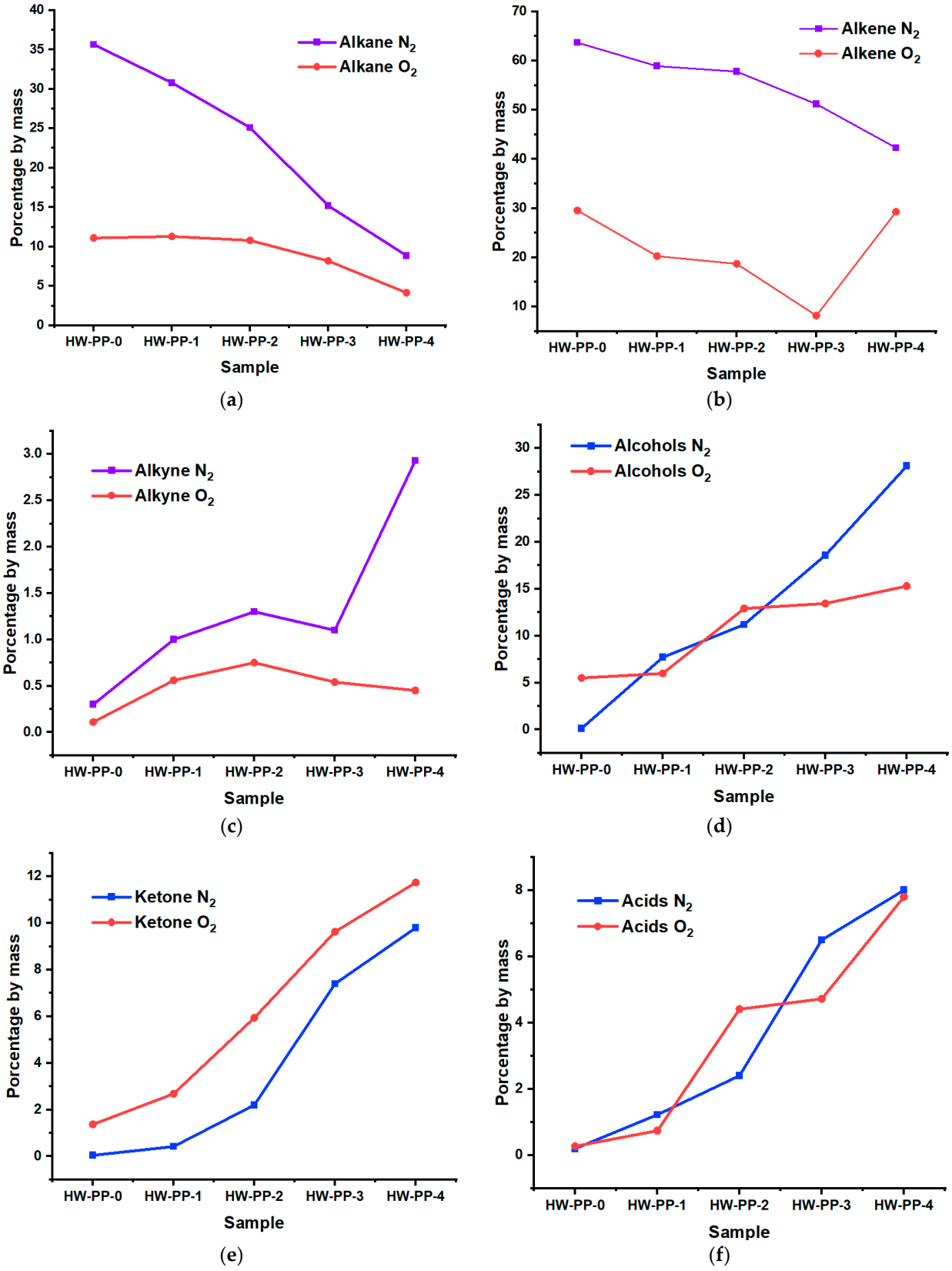

Figure 6. (**a**) Trend graph for alkanes in N_2 and O_2 atmospheres; (**b**) trend graph for alkenes in N_2 and O_2 atmospheres; (**c**) trend graph for alkynes in N_2 and O_2 atmospheres; (**d**) trend graph for alcohols in N_2 and O_2 atmospheres; (**e**) trend graph for ketones in N_2 and O_2 atmospheres; (**f**) trend graph for acids in N_2 and O_2 atmospheres.

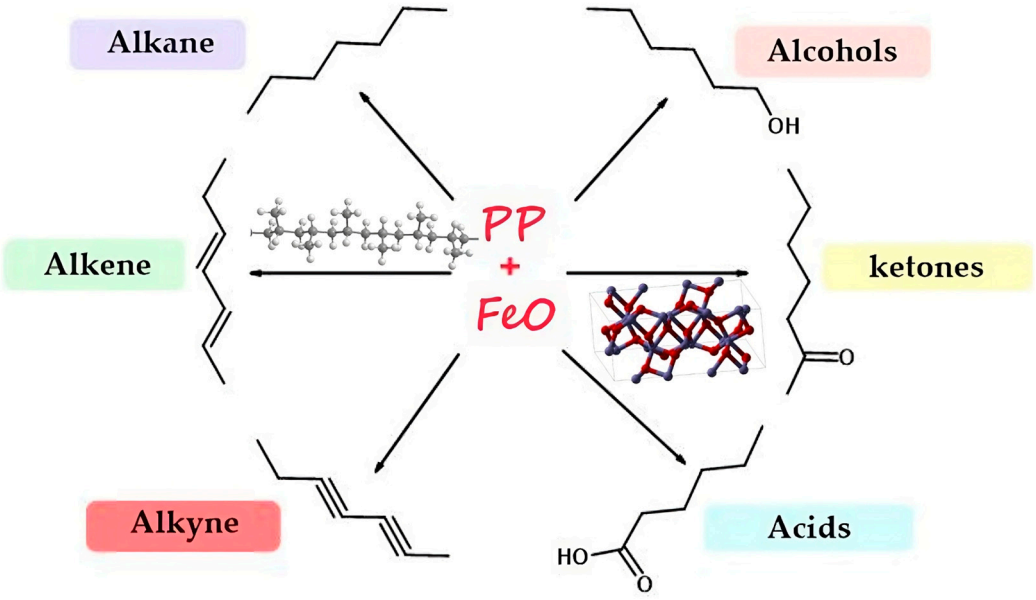

Figure 7. Diagram of products obtained by HPW pyrolysis.

3.4. Possible Reaction Mechanism

A possible reaction mechanism for the degradation of PP containing FeO as a catalyst is as follows. FeO is a non-stoichiometric solid, which implies that Fe^{+3} ions can exist in its crystal lattice, substituting Fe^{+2} ions [39,40,60]. The Fe^{+3} ions of Fe_2O_3 have high catalytic activity in low proportions (0.18%), reducing the activation energy and transforming free radicals into non-radical products [61]. Since the oxidation state of the metal generates this effect, it is intuited that the same happens with FeO. Figure 6 shows the standard degradation mechanism of PP, and Figures 8 and 9 show the degradation mechanism of PP in the presence of FeO. The pattern of these values suggests that iron oxide (FeO) experiences breakdown reactions that result in the generation of free radicals, including an ethyl radical, and these radicals react quickly with the polymer to speed up its deterioration. The effect of the ethyl radical at the beginning of the PP degradation is represented in Figure 10. This radical extracts hydrogen to form a tertiary radical, which then reacts with oxygen to give rise to a PP-peroxy radical. In turn, it extracts hydrogen from a nearby chain to give PP hydroperoxide, which is then hemolytically cleaved to give a PP alkoxy radical. IR and NMR have been used to discuss this mechanism for years [62–64]. As a result of homolysis, which releases a PP radical at the end of the chain, PP-methylketone is simultaneously formed, which gives rise to the following reactions: ethyl radical with PP-methylketone.

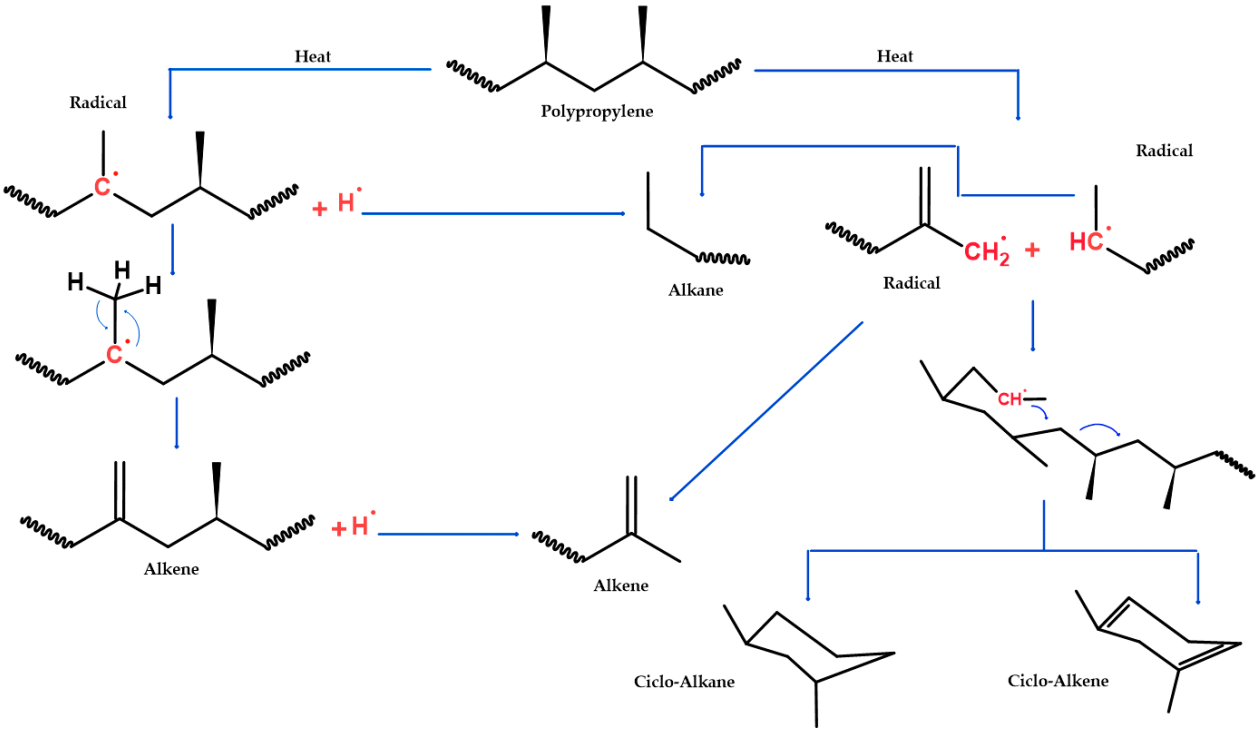

Figure 8. Thermal degradation of PP without a catalyst (FeO).

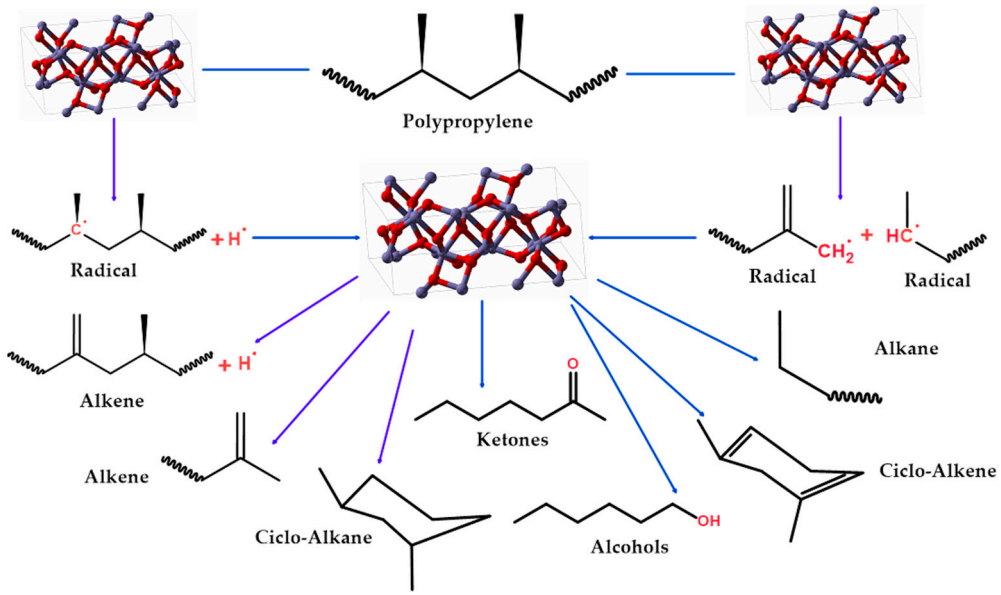

Figure 9. Thermal degradation of PP with catalyst (FeO).

In the free radicals of Figure 10, a hydrogen atom is abstracted from the tertiary atom near the carbonyl of PP-methylketone, displacing the reactive site and causing oxidation to progress at the tertiary carbon [65–67]. Alternatively, the PP-peroxy radical at the chain end interacts with oxygen to produce PP-hydroperoxide, which then reacts with the PP-methyl ketone-alkoxy at the chain end to produce 2,4-pentanedione. The acetone radical is created by the homolytic cleavage of PP-methyl ketone-alkoxy by another tertiary carbon bond, which then combines with other radicals to create 1-hydroxy-2-pentanone, 2-pentanone, and acetone. Similar routes have already been suggested [68]. The PP radical

at the chain end reacts with O_2 to produce the PP-hydroperoxide radical, which is followed by the PP-alkoxy radical, producing formaldehyde and PP-aldehyde, which continues oxidizing in the presence of O_2 to produce carboxylic acids such as formic acid and acetic acid. The latter has the PP-carbonyl radical by reacting with the ethyl radical, which in turn causes homolytic reactions and oxidation to produce CO and CO_2 Isobutylene, a molecule found in the degassing column, which also undergoes a radical reaction with the radical hydroxyl, followed by oxidation, to make the alkoxy radical. This radical then undergoes homolytic cleavages and reactions with the hydrogen radical to produce acetone, methanol, 1,2-isobutanediol, and 1-hydroxy-2-propanone. This final approach is an additional means of obtaining these valuable alcohols and ketones [69,70]. During the PP production processes, these molecules could enter as impurities, derived from some additives or formed by secondary reactions [71–79].

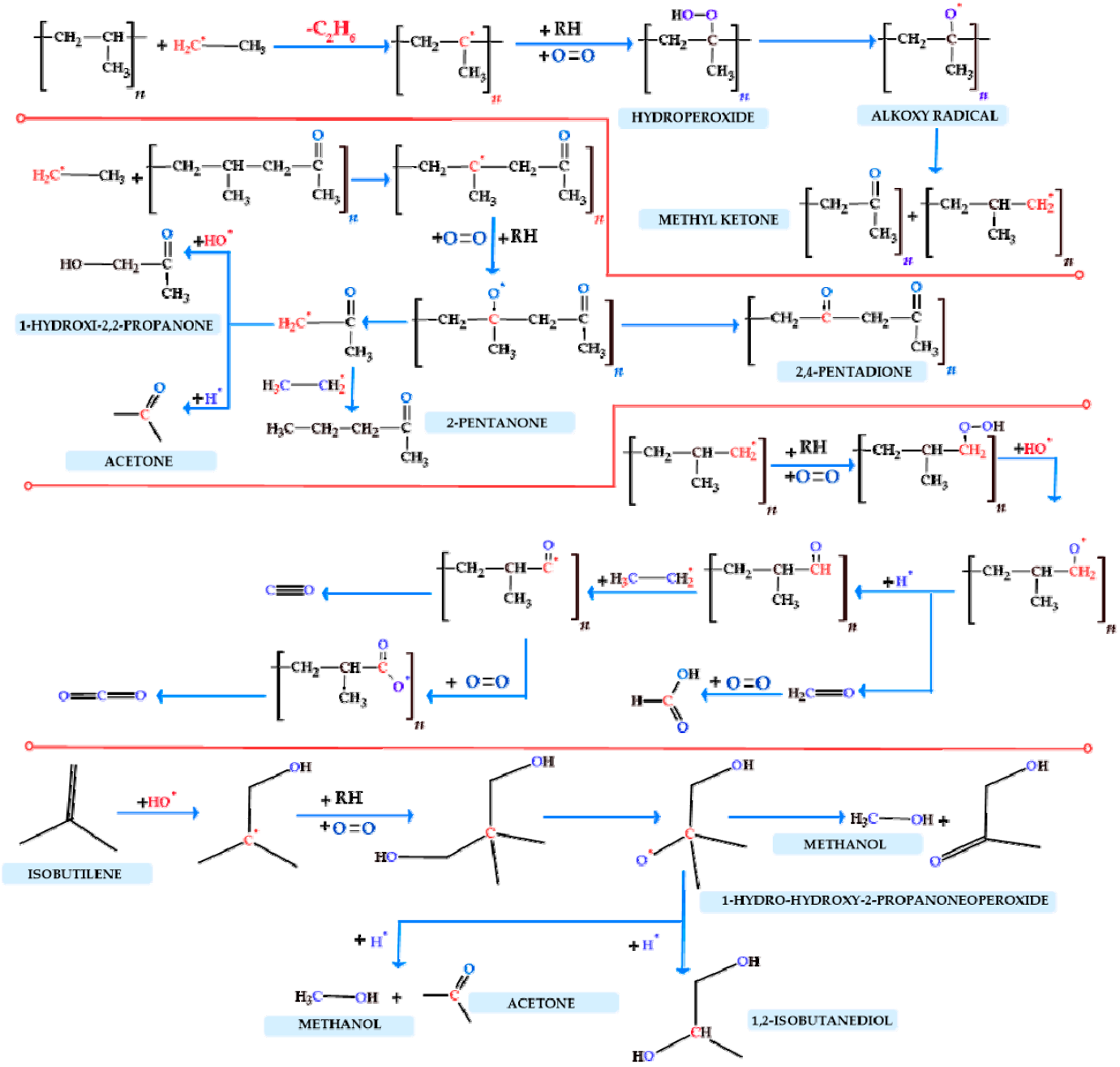

Figure 10. Thermal degradation of PP with catalyst (FeO) and traces of air (O_2).

3.5. Catalyst Presence

Chemical catalysts serve to accelerate the chemical reactions in the pyrolysis system. These catalysts are widely employed in manufacturing and are being researched to enhance product distribution and selectivity. Fast polymer pyrolysis utilizes catalysts such as kaolin and various zeolites. Catalytic degradation yields high-value products such as automotive fuels and C2–C4 olefins. When using FeO as a catalyst for medical waste pyrolysis, the activation energy of the mechanism and the optimized process temperature are reduced, accelerating the reaction rate. FeO's presence during pyrolysis also helps produce high-quality products with low energy consumption, which is crucial for cost-effective industrial applications. GC-MS analysis results indicate that metal oxides (FeO) have a limited catalytic effect on cracking other pyrolysis products, modestly favoring the formation of olefins and aromatics (Figure 11).

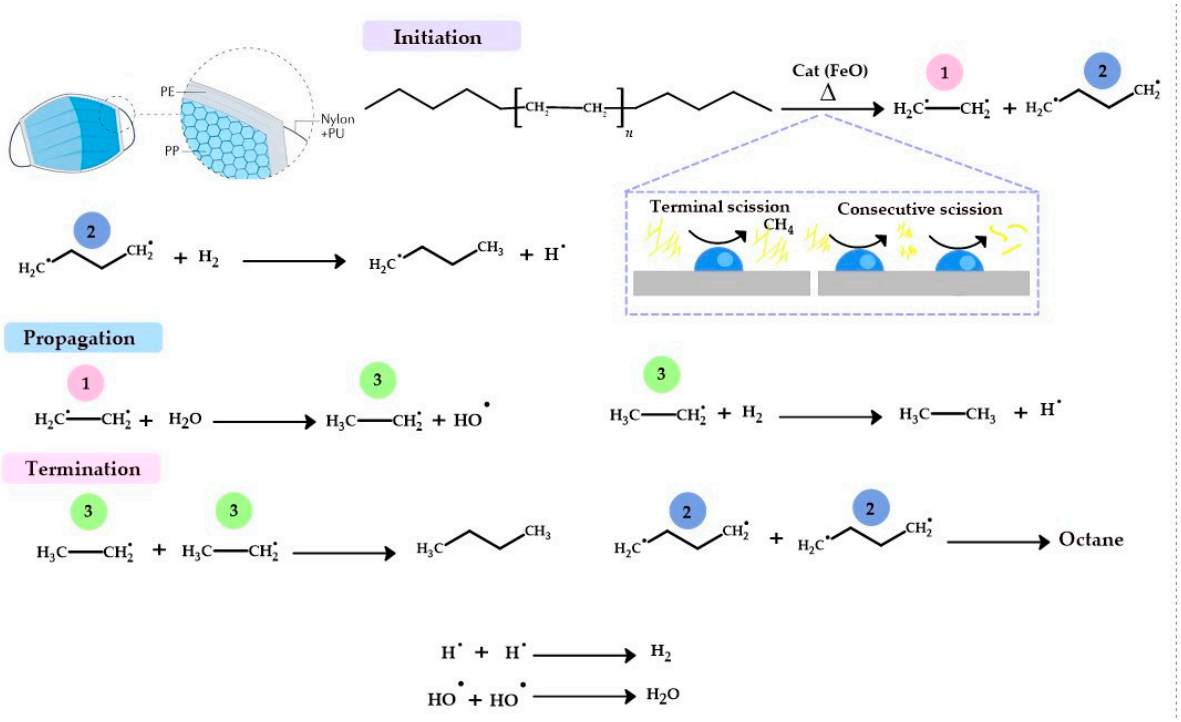

Figure 11. Pyrolysis, cracking, and deactivation of polypropylene under the influence of the FeO catalyst.

4. Conclusions

Utilizing FeO catalysts derived from industrial waste offers a sustainable solution for the pyrolysis and oxidation of hospital polypropylene in Cartagena, with significant implications for waste management and public health. Our findings indicate that FeO catalysts effectively facilitated the degradation of polypropylene, potentially contaminated with infectious diseases, through pyrolysis and oxidation processes. Specifically, higher FeO concentrations increased alkynes, alcohols, ketones, and carboxylic acids, while lower concentrations resulted in higher proportions of alkanes and alkenes. The formation of oxidized compounds, such as alcohols, ketones, and carboxylic acids, suggests creating conditions that could be hostile to the survival of pathogenic microorganisms, potentially reducing the risk of disease transmission associated with hospital waste. Additionally, by simplifying the composition of the waste, this approach could contribute to more effective waste management in healthcare facilities.

Author Contributions: Conceptualization, J.H.-F.; methodology, J.H.-F. and J.L.M.; validation, J.L.M. and J.H.-F.; formal analysis, J.H.-F.; investigation, J.L.M., J.C.S. and J.H.-F.; writing—original draft preparation, J.C.S.; writing—review and editing, J.C.S., J.L.M. and J.H.-F.; supervision, J.H.-F.

and J.C.S.; project administration, J.H.-F. All authors have read and agreed to the published version of the manuscript.

Funding: This research received no external funding.

Institutional Review Board Statement: Not applicable.

Informed Consent Statement: Not applicable.

Data Availability Statement: Data are contained within the article.

Conflicts of Interest: The authors declare no conflict of interest.

References

1. Rajmohan, K.V.S.; Ramya, C.; Viswanathan, M.R.; Varjani, S. Plastic pollutants: Effective waste management for pollution control and abatement. *Curr. Opin. Environ. Sci. Health* **2019**, *12*, 72–84. https://doi.org/10.1016/J.COESH.2019.08.006.
2. Windfeld, E.S.; Brooks, M.S.L. Medical waste management—A review. *J. Environ. Manag.* **2015**, *163*, 98–108. https://doi.org/10.1016/J.JENVMAN.2015.08.013.
3. PlasticsEurope. *Plastics-the Facts 2016 An Analysis of European Plastics Production, Demand and Waste Data*; PlasticsEurope: Brussels, Belgium, 2016.
4. Hahladakis, J.N.; Velis, C.A.; Weber, R.; Iacovidou, E.; Purnell, P. An overview of chemical additives present in plastics: Migration, release, fate and environmental impact during their use, disposal and recycling. *J. Hazard. Mater.* **2018**, *344*, 179–199. https://doi.org/10.1016/J.JHAZMAT.2017.10.014.
5. Geyer, R.; Jambeck, J.R.; Law, K.L. Production, use, and fate of all plastics ever made. *Sci. Adv.* **2017**, *3*, e1700782. https://doi.org/10.1126/SCIADV.1700782.
6. Zheng, J.; Suh, S. Strategies to reduce the global carbon footprint of plastics. *Nat. Clim. Chang.* **2019**, *9*, 374–378. https://doi.org/10.1038/s41558-019-0459-z.
7. Jambeck, J.R.; Geyer, R.; Wilcox, C.; Siegler, T.R.; Perryman, M.; Andrady, A.; Narayan, R.; Law, K.L. Plastic waste inputs from land into the ocean. *Science* **2015**, *347*, 768–771. https://doi.org/10.1126/SCIENCE.1260352/SUPPL_FILE/JAMBECK.SM.PDF.
8. MacKenzie, D. COVID-19 goes global. *New Sci.* **2020**, *245*, 7. https://doi.org/10.1016/S0262-4079(20)30424-3.
9. Babaji, P.; Singh, A.; Lau, H.; Lamba, G.; Somasundaram, P. Deletion of short arm of chromosome 18, Del(18p) syndrome. *J. Indian Soc. Pedod. Prev. Dent.* **2014**, *32*, 68–70. https://doi.org/10.4103/0970-4388.127063.
10. Selvaraj, D.; Raja, J.; Prasath, S. Interdisciplinary approach for bilateral maxillary canine: First premolar transposition with complex problems in an adult patient. *J. Pharm. Bioallied Sci.* **2013**, *5* (Suppl. 2), S190–S194. https://doi.org/10.4103/0975-7406.114319.
11. Liu, H.C.; You, J.X.; Lu, C.; Chen, Y.Z. Evaluating health-care waste treatment technologies using a hybrid multi-criteria decision making model. *Renew. Sustain. Energy Rev.* **2015**, *41*, 932–942. https://doi.org/10.1016/J.RSER.2014.08.061.
12. Yu, H.; Sun, X.; Solvang, W.D.; Zhao, X. Reverse Logistics Network Design for Effective Management of Medical Waste in Epidemic Outbreaks: Insights from the Coronavirus Disease 2019 (COVID-19) Outbreak in Wuhan (China). *Int. J. Environ. Res. Public Health* **2020**, *17*, 1770. https://doi.org/10.3390/IJERPH17051770.
13. Kumar, N.M.; Mohammed, M.A.; Abdulkareem, K.H.; Damasevicius, R.; Mostafa, S.A.; Maashi, M.S.; Chopra, S.S. Artificial intelligence-based solution for sorting COVID related medical waste streams and supporting data-driven decisions for smart circular economy practice. *Process Saf. Environ. Prot.* **2021**, *152*, 482–494. https://doi.org/10.1016/J.PSEP.2021.06.026.
14. Ilyas, S.; Srivastava, R.R.; Kim, H. Disinfection technology and strategies for COVID-19 hospital and bio-medical waste management. *Sci. Total Environ.* **2020**, *749*, 141652. https://doi.org/10.1016/J.SCITOTENV.2020.141652.
15. Dharmaraj, S.; Ashokkumar, V.; Pandiyan, R.; Munawaroh, H.S.H.; Chew, K.W.; Chen, W.-H.; Ngamcharussrivichai, C. Pyrolysis: An effective technique for degradation of COVID-19 medical wastes. *Chemosphere* **2021**, *275*, 130092. https://doi.org/10.1016/J.CHEMOSPHERE.2021.130092.
16. Cities Wonder Whether Recycling Counts as Essential During the Virus—Bloomberg. Available online: https://www.bloomberg.com/news/articles/2020-03-27/cities-wonder-whether-recycling-counts-as-essential-during-the-virus (accessed on 30 May 2024).
17. Ramadhani, B.; Kivevele, T.; Kihedu, J.H.; Jande, Y.A.C. Catalytic tar conversion and the prospective use of iron-based catalyst in the future development of biomass gasification: A review. *Biomass Convers. Biorefin.* **2020**, *12*, 1369–1392. https://doi.org/10.1007/S13399-020-00814-X.
18. Yao, D.; Wang, C.H. Pyrolysis and in-line catalytic decomposition of polypropylene to carbon nanomaterials and hydrogen over Fe- and Ni-based catalysts. *Appl. Energy* **2020**, *265*, 114819. https://doi.org/10.1016/J.APENERGY.2020.114819.
19. Jin, L.; Si, H.; Zhang, J.; Lin, P.; Hu, Z.; Qiu, B.; Hu, H. Preparation of activated carbon supported Fe–Al2O3 catalyst and its application for hydrogen production by catalytic methane decomposition. *Int. J. Hydrogen Energy* **2013**, *38*, 10373–10380. https://doi.org/10.1016/J.IJHYDENE.2013.06.023.
20. Xu, L.; Lin, X.; Xi, Y.; Lu, X.; Wang, C.; Liu, C. Alumina-supported Fe catalyst prepared by vapor deposition and its catalytic performance for oxidative dehydrogenation of ethane. *Mater. Res. Bull.* **2014**, *59*, 254–260. https://doi.org/10.1016/J.MATERRESBULL.2014.07.023.

21. Yao, D.; Li, H.; Dai, Y.; Wang, C.H. Impact of temperature on the activity of Fe-Ni catalysts for pyrolysis and decomposition processing of plastic waste. *Chem. Eng. J.* **2021**, *408*, 127268. https://doi.org/10.1016/J.CEJ.2020.127268.
22. Kumagai, S.; Hosaka, T.; Kameda, T.; Yoshioka, T. Removal of toxic HCN and recovery of H2-rich syngas via catalytic reforming of product gas from gasification of polyimide over Ni/Mg/Al catalysts. *J. Anal. Appl. Pyrolysis* **2017**, *123*, 330–339. https://doi.org/10.1016/J.JAAP.2016.11.012.
23. Rodríguez, E.; Gutiérrez, A.; Palos, R.; Vela, F.J.; Arandes, J.M.; Bilbao, J. Fuel production by cracking of polyolefins pyrolysis waxes under fluid catalytic cracking (FCC) operating conditions. *Waste Manag.* **2019**, *93*, 162–172. https://doi.org/10.1016/J.WASMAN.2019.05.005.
24. Veses, A.; Sanahuja-Parejo, O.; Callén, M.S.; Murillo, R.; García, T. A combined two-stage process of pyrolysis and catalytic cracking of municipal solid waste for the production of syngas and solid refuse-derived fuels. *Waste Manag.* **2020**, *101*, 171–179. https://doi.org/10.1016/J.WASMAN.2019.10.009.
25. Williams, P.T. Hydrogen and Carbon Nanotubes from Pyrolysis-Catalysis of Waste Plastics: A Review. *Waste Biomass Valorization* **2021**, *12*, 1–28. https://doi.org/10.1007/S12649-020-01054-W/.
26. Cai, N.; Xia, S.; Li, X.; Xiao, H.; Chen, X.; Chen, Y.; Bartocci, P.; Chen, H.; Williams, P.T.; Yang, H. High-value products from ex-situ catalytic pyrolysis of polypropylene waste using iron-based catalysts: The influence of support materials. *Waste Manag.* **2021**, *136*, 47–56. https://doi.org/10.1016/J.WASMAN.2021.09.030.
27. Alptekin, F.M.; Celiktas, M.S. Review on Catalytic Biomass Gasification for Hydrogen Production as a Sustainable Energy Form and Social, Technological, Economic, Environmental, and Political Analysis of Catalysts. *ACS Omega* **2022**, *7*, 24918–24941. https://doi.org/10.1021/ACSOMEGA.2C01538/.
28. Hao, T.; Huang, Y.; Li, F.; Wu, Y.; Fang, L. Facet-dependent Fe(II) redox chemistry on iron oxide for organic pollutant transformation and mechanisms. *Water Res.* **2022**, *219*, 118587. https://doi.org/10.1016/J.WATRES.2022.118587.
29. Hu, J.; Poelman, H.; Marin, G.B.; Detavernier, C.; Kawi, S.; Galvita, V.V. FeO controls the sintering of iron-based oxygen carriers in chemical looping CO2conversion. *J. CO2 Util.* **2020**, *40*, 101216. https://doi.org/10.1016/J.JCOU.2020.101216.
30. Lu, Z.H.; Xu, Q. Intermediates of CO oxidation on iron oxides: An experimental and theoretical study. *J. Chem. Phys.* **2011**, *134*, 34305. https://doi.org/10.1063/1.3523648/983327.
31. Hernández-Fernández, J.; Castro-Suarez, J.R.; Toloza, C.A.T. Iron Oxide Powder as Responsible for the Generation of Industrial Polypropylene Waste and as a Co-Catalyst for the Pyrolysis of Non-Additive Resins. *Int. J. Mol. Sci.* **2022**, *23*, 11708. https://doi.org/10.3390/IJMS231911708.
32. Cai, N.; Xia, S.; Li, X.; Sun, L.; Bartocci, P.; Fantozzi, F.; Zhang, H.; Chen, H.; Williams, P.T.; Yang, H. Influence of the ratio of Fe/Al_2O_3 on waste polypropylene pyrolysis for high value-added products. *J. Clean. Prod.* **2021**, *315*, 128240. https://doi.org/10.1016/J.JCLEPRO.2021.128240.
33. Zheng, Y.; Cheng, Y.; Wang, Y.; Bao, F.; Zhou, L.; Wei, X.; Zhang, Y.; Zheng, Q. Quasicubic alpha-Fe_2O_3 nanoparticles with excellent catalytic performance. *J. Phys. Chem. B* **2006**, *110*, 3093–3097. https://doi.org/10.1021/JP056617Q.
34. Acomb, J.C.; Wu, C.; Williams, P.T. Effect of growth temperature and feedstock:catalyst ratio on the production of carbon nanotubes and hydrogen from the pyrolysis of waste plastics. *J. Anal. Appl. Pyrolysis* **2015**, *113*, 231–238. https://doi.org/10.1016/J.JAAP.2015.01.012.
35. Wu, C.; Nahil, M.A.; Miskolczi, N.; Huang, J.; Williams, P.T. Processing real-world waste plastics by pyrolysis-reforming for hydrogen and high-value carbon nanotubes. *Environ. Sci. Technol.* **2014**, *48*, 819–826. https://doi.org/10.1021/ES402488B.
36. Chen, X.; Liu, Z.; Chen, W.; Yang, H.; Chen, H. Catalytic pyrolysis of cotton stalk to produce aromatic hydrocarbons over Fe modified CaO catalysts and ZSM-5. *J. Anal. Appl. Pyrolysis* **2022**, *166*, 105635. https://doi.org/10.1016/J.JAAP.2022.105635.
37. Cho, D.W.; Chon, C.-M.; Yim, G.-J.; Ryu, J.; Jo, H.; Kim, S.-J.; Jang, J.-Y.; Song, H. Adsorption of potentially harmful elements by metal-biochar prepared via Co-pyrolysis of coffee grounds and Nano Fe(III) oxides. *Chemosphere* **2023**, *319*, 136536. https://doi.org/10.1016/J.CHEMOSPHERE.2022.136536.
38. Deng, J.; Deng, X.; Yuan, S.; Ma, D.; Liu, J.; Xie, X.; He, R.; Yang, T. Effect of precipitating agents for the preparation of Fe-based catalysts on coal pyrolysis: Effect of Ba and Mg additives. *Fuel* **2022**, *320*, 124000. https://doi.org/10.1016/J.FUEL.2022.124000.
39. Ge, L.; Zhao, C.; Zuo, M.; Du, Y.; Tang, J.; Chu, H.; Wang, Y.; Xu, C. Effects of Fe addition on pyrolysis characteristics of lignin, cellulose and hemicellulose. *J. Energy Inst.* **2023**, *107*, 101177. https://doi.org/10.1016/J.JOEI.2023.101177.
40. Dong, Y.; Tian, B.; Guo, F.; Du, S.; Zhan, Y.; Zhou, H.; Qian, L. Application of low-cost Fe-based catalysts in the microwave-assisted pyrolysis of macroalgae and lignocellulosic biomass for the upgradation of bio-oil. *Fuel* **2021**, *300*, 120944. https://doi.org/10.1016/J.FUEL.2021.120944.
41. He, R.; Liu, H.; Lu, Q.; Zhao, Y.; Wang, X.; Xie, X.; Deng, X.; Yuan, S. Effects of Si and Al elements in coal on Fe-catalyzed brown coal pyrolysis. *Fuel* **2022**, *315*, 123170. https://doi.org/10.1016/J.FUEL.2022.123170.
42. Yao, D.; Wu, C.; Yang, H.; Zhang, Y.; Nahil, M.A.; Chen, Y.; Williams, P.T.; Chen, H. Co-production of hydrogen and carbon nanotubes from catalytic pyrolysis of waste plastics on Ni-Fe bimetallic catalyst. *Energy Convers. Manag.* **2017**, *148*, 692–700. https://doi.org/10.1016/J.ENCONMAN.2017.06.012.
43. Aboul-Enein, A.A.; Awadallah, A.E. Production of nanostructured carbon materials using Fe–Mo/MgO catalysts via mild catalytic pyrolysis of polyethylene waste. *Chem. Eng. J.* **2018**, *354*, 802–816. https://doi.org/10.1016/J.CEJ.2018.08.046.
44. Tezel, E.; Figen, H.E.; Baykara, S.Z. Hydrogen production by methane decomposition using bimetallic Ni–Fe catalysts. *Int. J. Hydrogen Energy* **2019**, *44*, 9930–9940. https://doi.org/10.1016/J.IJHYDENE.2018.12.151.

45. Kwon, G.; Cho, D.W.; Kwon, E.E.; Rinklebe, J.; Wang, H.; Song, H. Beneficial use of Fe-impregnated bentonite as a catalyst for pyrolysis of grass cut into syngas, bio-oil and biochar. *Chem. Eng. J.* **2022**, *448*, 137502. https://doi.org/10.1016/J.CEJ.2022.137502.
46. Liu, R.; Li, C.; Zheng, J.; Liao, L.; Zhang, Y. Effect of Fe impregnation on CO_2-assisted pyrolysis of hazelnut shell. *Fuel* **2022**, *324*, 124514. https://doi.org/10.1016/J.FUEL.2022.124514.
47. Tafjord, J.; Regli, S.K.; Dugulan, A.I.; Rønning, M.; Rytter, E.; Holmen, A.; Myrstad, R.; Yang, J. Influence of temperature during pyrolysis of Fe-alginate: Unraveling the pathway towards highly active Fe/C catalysts. *Appl. Catal. A Gen.* **2022**, *644*, 118834. https://doi.org/10.1016/j.apcata.2022.118834.
48. Yuwen, C.; Liu, B.; Rong, Q.; Hou, K.; Zhang, L.; Guo, S. Mechanism of microwave-assisted iron-based catalyst pyrolysis of discarded COVID-19 masks. *Waste Manag.* **2023**, *155*, 77–86. https://doi.org/10.1016/J.WASMAN.2022.10.041.
49. Wang, H.; Zhang, B.; Luo, P.; Huang, K.; Zhou, Y. Simultaneous Achievement of High-Yield Hydrogen and High-Performance Microwave Absorption Materials from Microwave Catalytic Deconstruction of Plastic Waste. *Processes* **2022**, *10*, 782. https://doi.org/10.3390/PR10040782.
50. Jie, X.; Li, W.; Slocombe, D.; Gao, Y.; Banerjee, I.; Gonzalez-Cortes, S.; Yao, B.; AlMegren, H.; Alshihri, S.; Dilworth, J.; et al. Microwave-initiated catalytic deconstruction of plastic waste into hydrogen and high-value carbons. *Nat. Catal.* **2020**, *3*, 902–912. https://doi.org/10.1038/S41929-020-00518-5.
51. Álvarez, M.L.; Gascó, G.; Palacios, T.; Paz-Ferreiro, J.; Méndez, A. Fe oxides-biochar composites produced by hydrothermal carbonization and pyrolysis of biomass waste. *J. Anal. Appl. Pyrolysis* **2020**, *151*, 104893. https://doi.org/10.1016/J.JAAP.2020.104893.
52. Das, P.; Tiwari, P. The effect of slow pyrolysis on the conversion of packaging waste plastics (PE and PP) into fuel. *Waste Manag.* **2018**, *79*, 615–624. https://doi.org/10.1016/J.WASMAN.2018.08.021.
53. Sobko, A.A. Generalized van der Waals-Berthelot equation of state. *Dokl. Phys.* **2008**, *53*, 416. https://doi.org/10.1134/S1028335808080028.
54. Sapuan, S.M.; Jamal, T.; Abdan, K. Slow Pyrolysis of Disinfected COVID-19 Non-Woven Polypropylene (PP) Waste. 2021. Available online: https://www.researchgate.net/publication/351710043 (accessed on 31 May 2024).
55. Marcilla, A.; García-Quesada, J.C.; Sánchez, S.; Ruiz, R. Study of the catalytic pyrolysis behaviour of polyethylene–polypropylene mixtures. *J. Anal. Appl. Pyrolysis* **2005**, *74*, 387–392. https://doi.org/10.1016/J.JAAP.2004.10.005.
56. Jung, S.H.; Cho, M.H.; Kang, B.S.; Kim, J.S. Pyrolysis of a fraction of waste polypropylene and polyethylene for the recovery of BTX aromatics using a fluidized bed reactor. *Fuel Process. Technol.* **2010**, *91*, 277–284. https://doi.org/10.1016/J.FUPROC.2009.10.009.
57. Panda, A.K.; Singh, R.K.; Mishra, D.K. Thermolysis of waste plastics to liquid fuel: A suitable method for plastic waste management and manufacture of value added products—A world prospective. *Renew. Sustain. Energy Rev.* **2010**, *14*, 233–248. https://doi.org/10.1016/J.RSER.2009.07.005.
58. Ahmad, I.; Khan, M.I.; Khan, H.; Ishaq, M.; Tariq, R.; Gul, K.; Ahmad, W. Pyrolysis Study of Polypropylene and Polyethylene Into Premium Oil Products. *Int. J. Green Energy* **2015**, *12*, 663–671. https://doi.org/10.1080/15435075.2014.880146.
59. Aguado, J.; Serrano, D.P.; Escola, J.M.; Garagorri, E.; Fernández, J.A. Catalytic conversion of polyolefins into fuels over zeolite beta. *Polym. Degrad. Stab.* **2000**, *69*, 11–16. https://doi.org/10.1016/S0141-3910(00)00023-9.
60. Li, M.; Endo, R.; Akoshima, M.; Susa, M. Temperature Dependence of Thermal Diffusivity and Conductivity of FeO Scale Produced on Iron by Thermal Oxidation. *ISIJ Int.* **2017**, *57*, 2097–2106. https://doi.org/10.2355/isijinternational.ISIJINT-2017-301.
61. Nakatani, H.; Shibata, H.; Miyazaki, K.; Yonezawa, T.; Takeda, H.; Azuma, Y.; Watanabe, S. Studies on heterogeneous degradation of polypropylene/talc composite: Effect of iron impurity on the degradation behavior. *J. Appl. Polym. Sci.* **2010**, *115*, 167–173. https://doi.org/10.1002/APP.31010.
62. Mowery, D.M.; Assink, R.A.; Derzon, D.K.; Klamo, S.B.; Clough, R.L.; Bernstein, R. Solid-state 13C NMR investigation of the oxidative degradation of selectively labeled polypropylene by thermal aging and γ-irradiation. *Macromolecules* **2005**, *38*, 5035–5046. https://doi.org/10.1021/MA047381B.
63. Carlsson, D.J.; Wiles, D.M. The Photooxidative Degradation of Polypropylene. Part I. Photooxidation and Photoinitiation Processes. *J. Macromol. Sci. Part C Polym. Rev.* **1976**, *14*, 65–106. https://doi.org/10.1080/15321797608076113.
64. Bahri-Laleh, N.; Correa, A.; Mehdipour-Ataei, S.; Arabi, H.; Haghighi, M.N.; Zohuri, G.; Cavallo, L. Moving up and down the titanium oxidation state in Ziegler-Natta catalysis. *Macromolecules* **2011**, *44*, 778–783. https://doi.org/10.1021/MA1023582.
65. Lee, H.W.; Park, Y.K. Catalytic Pyrolysis of Polyethylene and Polypropylene over Desilicated Beta and Al-MSU-F. *Catalysts* **2018**, *8*, 501. https://doi.org/10.3390/CATAL8110501.
66. Papuga, S.; Djurdjevic, M.; Ciccioli, A.; Ciprioti, S.V. Catalytic Pyrolysis of Plastic Waste and Molecular Symmetry Effects: A Review. *Symmetry* **2023**, *15*, 38. https://doi.org/10.3390/SYM15010038.
67. Clough, R.L. Isotopic exchange in gamma-irradiated mixtures of C24H5 and C24D5: Evidence of free radical migration in the solid state. *J. Chem. Phys.* **1987**, *87*, 1588–1595. https://doi.org/10.1063/1.453218.
68. Commereuc, S.; Vaillant, D.; Philippart, J.L.; Lacoste, J.; Lemaire, J.; Carlsson, D.J. Photo and thermal decomposition of iPP hydroperoxides. *Polym. Degrad. Stab.* **1997**, *57*, 175–182. https://doi.org/10.1016/S0141-3910(96)00183-8.
69. Suriapparao, D.V.; Gautam, R.; Jeeru, L.R. Analysis of pyrolysis index and reaction mechanism in microwave-assisted ex-situ catalytic co-pyrolysis of agro-residual and plastic wastes. *Bioresour. Technol.* **2022**, *357*, 127357. https://doi.org/10.1016/J.BIORTECH.2022.127357.

70. Zhang, Y.; Fu, Z.; Wang, W.; Ji, G.; Zhao, M.; Li, A. Kinetics, Product Evolution, and Mechanism for the Pyrolysis of Typical Plastic Waste. *ACS Sustain. Chem. Eng.* **2022**, *10*, 91–103. https://doi.org/10.1021/ACSSUSCHEMENG.1C04915.
71. Hernández-Fernández, J.; Vivas-Reyes, R.; Toloza, C.A.T. Experimental Study of the Impact of Trace Amounts of Acetylene and Methylacetylene on the Synthesis, Mechanical and Thermal Properties of Polypropylene. *Int. J. Mol. Sci*. **2022**, *23*, 12148.
72. Hernández-Fernández, J.; Cano, H.; Aldas, M. Impact of Traces of Hydrogen Sulfide on the Efficiency of Ziegler–Natta Catalyst on the Final Properties of Polypropylene. *Polymers* **2022**, *14*, 3910.
73. Hernández-Fernández, J.; Lopez-Martinez, J.; Barceló, D. Development and validation of a methodology for quantifying partsper-billion levels of arsine and phosphine in nitrogen, hydrogen and liquefied petroleum gas using a variable pressure sampler coupled to gas chromatography-mass spectrometry. *J. Chromatogr. A* **2021**, *1637*, 461833.
74. Pavon, C.; Aldas, M.; Hernández-Fernández, J.; López-Martínez, J. Comparative characterization of gum rosins for their use as sustainable additives in polymeric matrices. *J. Appl. Polym. Sci*. **2021**, *139*, 51734.
75. Hernandez-Fernández, J.; Guerra, Y.; Espinosa, E. Development and Application of a Principal Component Analysis Model to Quantify the Green Ethylene Content in Virgin Impact Copolymer Resins During Their Synthesis on an Industrial Scale. *J. Polym. Environ*. **2022**, *30*, 4800–4808.
76. Chacon, H.; Cano, H.; Fernández, J.H.; Guerra, Y.; Puello-Polo, E.; Ríos-Rojas, J.F.; Ruiz, Y. Effect of Addition of Polyurea as an Aggregate in Mortars: Analysis of Microstructure and Strength. *Polymers* **2022**, *14*, 1753.
77. Hernández-Fernández, J.; González-Cuello, R.; Ortega-Toro, R. Parts per million of propanol and arsine as responsible for the poisoning of the propylene polymerization reaction. *Polymers* **2023**, *15*, 3619. https://doi.org/10.3390/POLYM15173619.
78. Hernández-Fernández, J.; Ortega-Toro, R.; Castro-Suarez, J.R. Theoretical–experimental study of the action of trace amounts of formaldehyde, propionaldehyde, and butyraldehyde as inhibitors of the ziegler–natta catalyst and the synthesis of an ethylene–propylene copolymer. *Polymers* **2023**, *15*, 1098. https://doi.org/10.3390/POLYM15051098.
79. Hernandez-Fernandez, J.; Cano, H.; Guerra, Y. Detection of Bisphenol A and Four Analogues in Atmospheric Emissions in Petrochemical Complexes Producing Polypropylene in South America. *Molecules* **2022**, *27*, 4832. https://doi.org/10.3390/molecules27154832.